INORGANIC CHEMISTRY FRONTIERS

RESEARCH ARTICLE

View Article Online
View Journal | View Issue

Cite this: *Inorg. Chem. Front.*, 2025, **12**, 4272

Urea-induced platelike ZSM-5 zeolites with Si zoning for efficient alkylation of toluene with ethanol to *para*-ethyltoluene†

Jialin Tan,‡[a] Lei Miao,‡[b,c] Yang Liu,[d] Shujing Chen,[a] Zhe Hong,*[a] Lihua Deng,[a] Qun Yang,[a] Xianlong Gao,[b] Fangtao Huang*[b] and Zhirong Zhu*[b]

Received 10th January 2025,
Accepted 23rd March 2025

DOI: 10.1039/d5qi00100e

rsc.li/frontiers-inorganic

Platelike zeolites with a short diffusion pathway are promising catalysts due to mass transfer advantages. Herein, platelike ZSM-5 with a reduced *b*-axis thickness (~90 nm) was synthesized using a urea-assisted crystallization strategy. We disclose the significant application of this platelike catalyst in the toluene alkylation reaction with ethanol to produce *para*-ethyltoluene (*p*-ET). The reaction results demonstrate that this platelike ZSM-5 exhibits a higher toluene conversion (58.3%) and ET selectivity (88.7%) than conventional ZSM-5. This improvement is primarily due to the shortened straight channels of platelike ZSM-5, which facilitate mass transport and increase the accessibility to acid sites. Nevertheless, the shortened *b*-axis of platelike ZSM-5 seems to have no significant positive impact on *para*-selectivity for *p*-ET. Hence, we constructed a Si-zoned external surface on the platelike ZSM-5 by means of the surface modification strategy to accurately passivate the surface acid sites, thereby inhibiting the isomerization reaction, and achieving higher selectivity for *p*-ET (>95%) and extended catalytic stability (>100 h) in the reaction of toluene alkylation with ethanol.

1 Introduction

para-Ethyltoluene (*p*-ET) is an important chemical used in the production of commercial polymers, agriculture, and other materials with significant applications.[1,2] In recent years, the excessive capacity of toluene in the petrochemical industry has made the alkylation of toluene with inexpensive and easily available ethanol to produce *p*-ET very significant, promoting the high value-added utilization of aromatic hydrocarbons. ZSM-5 zeolites, with tunable acidity, characteristic pore structures, and excellent hydrothermal stability, are commonly used as catalysts for the alkylation of toluene with ethanol.[3,4] However, the ethyltoluene (ET) isomers in the alkylation product were distributed according to thermodynamic equilibrium (*p*-ET (25.9%), *meta*-ethyltoluene (*m*-ET, 59.3%), and *ortho*-ethyltoluene (*o*-ET, 14.8%)) on the conventional ZSM-5,[5] which necessitates a costly and energy-intensive process to separate *p*-ET from the isomers with close boiling points. The acid properties of ZSM-5 play an indispensable role in determining the catalytic performance. However, the non-shape selective acid sites present on the external surface of zeolites are accountable for the low *p*-ET selectivity.[6,7] Due to the absence of spatial confinement, the external surface acid sites readily catalyze the isomerization of *p*-ET to form *m*-ET and *o*-ET. To realize higher shape selectivity, it is essential to passivate the surface acid sites using modifiers. These modifiers, such as phosphorus, MgO, boron, and SiO_2, serve as acid-site neutralizing reagents that chemisorb to the hydroxyl groups on zeolite surfaces.[8–10]

Besides the effects of acidity, the structural properties of the zeolites also play an indispensable role in determining the catalytic activity. ZSM-5 features a distinct framework with two sets of intersecting 10-membered ring (10MR) channels, *i.e.* one set of straight channels (0.52 × 0.58 nm) parallel to the *b*-axis and the other set of sinusoidal channels (0.51 × 0.55 nm) parallel to the *a*-axis.[11,12] The long channels would lead to the enrichment of ethanol, which favors side reactions such as ethanol dehydration or ethanol deep decomposition. These lead to low ethanol utilization efficiency and *p*-ET selectivity, as well as rapid catalyst deactivation.[13,14] This problem can be partially circumvented by reducing the path length through the zeolite crystal. Recently, the *b*-axis-oriented ZSM-5 crystals have attracted extensive attention owing to their

[a]*College of Biological, Chemical Sciences and Engineering, Jiaxing University, Jiaxing, Zhejiang, 314001, China. E-mail: 1961268317@qq.com*
[b]*School of Chemical Science and Engineering, Tongji University, Shanghai 200092, China. E-mail: FangtaoHuang1993@163.com, zhuzhirong@tongji.edu.cn*
[c]*Guangzhou Institute for Food Inspection, Guangzhou, 511400, China*
[d]*International Innovation Institute, Beihang University, Hangzhou, 311115, China*
†Electronic supplementary information (ESI) available. See DOI: https://doi.org/10.1039/d5qi00100e
‡These authors contributed equally to this work.

advantages of the shortened *b*-axis, thereby providing a short diffusion path along the straight channels. It provides excellent catalytic performance in a wide range of relevant catalytic processes, including the methanol-to-hydrocarbon (MTH),[15,16] methanol to propylene (MTP),[17] ring alkylation of benzene with methanol,[18,19] catalytic cracking,[20] and other diffusion-restricted reactions.[21,22] These inspiring findings have provided guidelines to solve the diffusion limitations of conventional ZSM-5 by shortening the diffusion path. Despite great promise, its application in the alkylation of toluene with ethanol has been rarely studied. It has been reported that adding synthesis modifiers to the starting gel could substantially change the zeolite crystal morphology.[45] In particular, urea can be spontaneously dispersed on the (010) MFI surface owing to favorable energetic factors, thereby controlling the growth of the zeolite along the *b*-axis.[46]

Herein, we report a urea-assisted crystallization strategy to fabricate a series of platelike ZSM-5 crystals with a controllable *b*-axis thickness (90–300 nm) by adjusting the dosage of urea. The toluene alkylation performances of these catalysts with different *b*-axis thicknesses are systematically compared, as the thinner platelike ZSM-5 (Z5-0.18) exhibits higher activity, which is primarily attributed to the shortened straight channels and decreased diffusion resistance. Interestingly, N species seems to be unexpectedly introduced into Z5-0.18 due to the presence of urea, thereby modulating the acid properties. Moreover, the surface modification strategy was developed to passivate the external acid sites *via* constructing a Si-zoned external surface on platelike ZSM-5, enabling long-term stable operation with over 95% *p*-ET selectivity.

2 Experimental

2.1 Catalyst preparation

Synthesis of platelike ZSM-5. Platelike ZSM-5 samples were prepared *via* a hydrothermal crystallization process.[23,24] Typically, sodium aluminate ($NaAlO_2$) was dissolved in distilled water, followed by the addition of 25% tetrapropylammonium hydroxide (TPAOH), tetraethyl orthosilicate (TEOS), and urea under vigorous stirring. The molar composition of the precursor gel was $SiO_2 : Al_2O_3 : TPAOH : H_2O :$ urea = $1 : 0.01 : 1.8 : 12 : x$, (x = 0, 0.09, and 0.18). Subsequently, the precursor gel was loaded into a Teflon-lined autoclave and heated at 180 °C for 48 h under stirring. The solid product was obtained by filtration, washing, and drying, and then it was calcined at 550 °C for 6 h to remove the template. The NH_4-type zeolites were prepared by ion-exchange with an aqueous solution of ammonium nitrate (four times) at 95 °C for 4 h, followed by calcining at 550 °C for 2 h to obtain the H-type ZSM-5 zeolite. The resulting H-type ZSM-5 samples were denoted as "Z5-*x*", where *x* represents the molar ratio of urea.

2.2 Surface modification

Synthesis of SiO_2 modified ZSM-5 (*y*-Si-Z5). SiO_2 surface modified ZSM-5 catalysts were prepared by the chemical liquid phase deposition (CLD) method.[25] Typically, 10 g of the Z5-0.18 catalyst was added to the mixture solution of 100 g hexane and 10.42 g TEOS, and then stirred for 4 h. The obtained product was dried at 110 °C overnight and calcined at 550 °C for 2 h. One cycle of CLD modification is effective at coating ~4.0% SiO_2 on the zeolite. The surface modification procedure was conducted 1–3 times to obtain samples with different SiO_2 loadings. The final catalysts were denoted as "*y*-Z5-0.18", where *y* is the number of SiO_2-CLD modification times.

A detailed description of the catalyst characterization and catalytic testing conducted on the prepared samples is shown in the ESI.†

3 Results and discussion

3.1 Structural properties

The ZSM-5 samples with different *b*-axis thicknesses were synthesized *via* a hydrothermal process in urea medium by adjusting the urea amount. Detailed synthesis conditions are reported in the "Catalyst preparation" section. Scanning electron microscopy (SEM) images show that the samples of Z5-0, Z5-0.09 and Z5-0.18 exhibit evidently diverse morphology (Fig. 1a–c). The Z5-0.18 sample exhibits a well-formed platelike morphology, whereas the Z5-0 sample exhibits a typical rounded-boat morphology. This might be caused by the adsorption of urea and its interaction with the (010) planes in aqueous systems, thereby inhibiting the crystal growth along the *b*-axis.[26,27] Atomic force microscopy (AFM) images also demonstrate that the platelike crystals of Z5-0.18 exhibit a smaller *b*-axis thickness (~90 nm) than the Z5-0 sample (Fig. 1h and i), which is in accordance with the SEM results. The platelike morphology of Z5-0.18 can also be confirmed by transmission electron microscopy (TEM) images (Fig. 1d). Moreover, the selected area electron diffraction (SAED) pattern and atomic-resolution high-angle annular dark-field scanning transmission electron microscopy (HAADF-STEM) images of Z5-0.18 clearly demonstrate a typical MFI straight channel along the *b*-axis, which proves that the platelike surfaces are parallel to the (010) planes (Fig. 1e and f). In addition, HADDF and EDS mapping images of Z5-0.18 reveal that Si and O elements are homogeneously distributed on the entire surface of zeolite (Fig. 1g). Interestingly, there are discriminable N signals in elemental mappings (pink). We speculate that the N species might be doped into the zeolite after the hydrothermal and calcination process in the presence of urea as the nitrogen source.

Concerned about the introduction of N *via* a hydrothermal process in the presence of urea, the chemical nature of the N species is analyzed by XPS N 1s spectra (Fig. 2). As for the Z5-0 sample (without urea), there are only very weak signals of N species at around 401.8 eV, which can be assigned to the chemisorbed nitrogen. Whereas the other two samples of Z5-0.09 and Z5-0.18 (urea present) exhibit prominent N signals at around 402.8 eV, which belongs to Si–N bonding (such as Si-NH-Si, Si-NH-Al or Si-NH2 groups).[44] To further identify the N

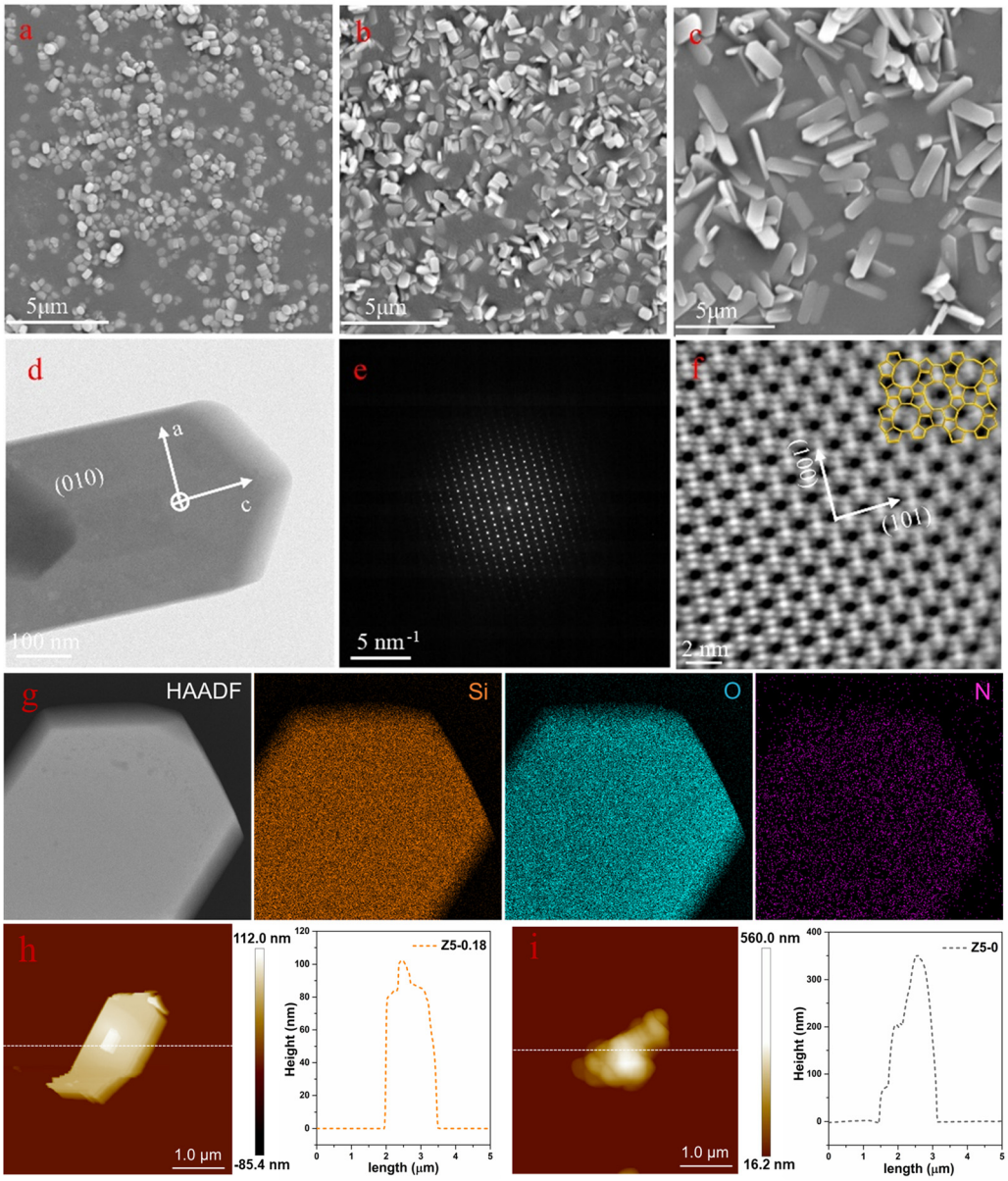

Fig. 1 General structural features of ZSM-5 catalysts with different *b*-axis thicknesses. (a–c) SEM images of (a) Z5-0; (b) Z5-0.09; and (c) Z5-0.18. (d) TEM images, (e) SAED pattern and (f) AC-HAADF-STEM images of the Z5-0.18 sample. (g) HADDF and EDS mapping images of Z5-0.18: Si (orange), O (blue) and N (pink). AFM images and the corresponding height profiles of (h) Z5-0.18 sample and (i) Z5-0 sample.

location, the crystal of Z5-0.18 is chopped out using a focused ion beam (FIB) along the *b*-axis orientation (Fig. 3). The two cutting positions are marked, and the corresponding EDS mapping images of Z5-0.18 are also displayed in Fig. 3. It seems that the Z5-0.18 sample exhibits homogeneous N elemental distribution from the surface to the core of the zeolite. The above results imply that the N species introduced into zeolite mainly come from urea and the N species in Z5-0.18 seems to be introduced into both surface and inner cavity of the Z5-0.18 zeolite. The N species doping may restructure the surface Lewis acid–base pairs on zeolites and then boost the catalytic performance, as reported in our previous work.[7,31]

For further illustrating the morphological change among these catalysts, the length along the three axes and the aspect ratio between different faces on zeolites are investigated. With the increase of urea content, the ZSM-5 crystals grow from ~620 to ~1900 nm along the *c*-axis, whereas the thickness of the *b*-axis significantly decreases from ~300 to ~90 nm (Fig. 4a and Table 1). The ratio between the *c*-axis and *b*-axis (L_c/L_b) was used to evaluate the changes in the (100) and (010) faces, where the pore mouths of sinusoidal and straight channels were located, respectively. As shown in Fig. 4b, the L_c/L_b aspect ratio increased from ~2.1 to ~21.2, with the increase of the molar ratio of urea in the gel from 0 to 0.18, implying that the

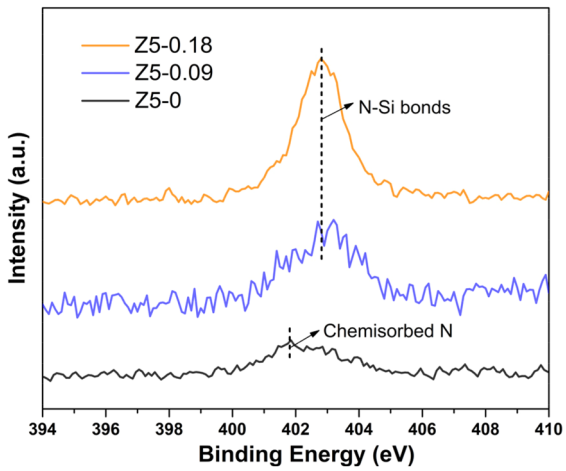

Fig. 2 N 1s XPS spectra of Z5-0, Z5-0.09 and Z5-0.18 catalysts.

growth in the *b* direction was greatly suppressed by the introduction of urea.

The XRD patterns of samples prepared with varying urea contents during hydrothermal synthesis, as shown in Fig. 4c, demonstrate the typical characteristic peaks of highly crystalline ZSM-5 (2θ = 7.9, 8.9, 23.2, 23.7, and 24.0°). Interestingly, the intensity ratio between 8.9° (010) and 7.9° (101) in the Z5-0.18 sample increased compared with that of the Z5-0 sample, indicating the enhanced diffraction along the (010) planes compared to the (101) planes in the zeolite crystals with the increase of the urea content. This effect is a consequence of the shortened *b*-axis thicknesses and a larger *c*-axis, as shown in Fig. 4a, b and Table 1. Combining the results of XRD and L_c/L_b, we considered that in the Z5-0.18 sample, the region perpendicular to the (010) crystal face along the *b*-axis becomes thinner, resulting in enhanced diffraction of the (010) crystal face. Moreover, a longer *c*-axis also results in a higher exposure degree of the (010) face.

Besides, the N_2 adsorption–desorption isotherms in Fig. 4d display typical type-I isotherms for all samples, revealing the microporous structures of the samples.[28] Different from the Z5-0 sample, both Z5-0.09 and Z5-0.18 show a noticeable capillary condensation step at a relative pressure of P/P_0 = 0.1–0.2. This should be attributed to a fluid-to-crystalline-like phase transition of the adsorbed phase in the micropore of ZSM-5 zeolites with a high Si/Al ratio.[27,28] Notably, the microporous surface area (S_{micro}) and volume (V_{micro}) of these samples are closely similar. It indicates that the introduction of urea during the hydrothermal process did not alter the intrinsic microporous structure of ZSM-5, although the morphology did change. Nevertheless, the external specific surface area (S_{ext}) and total pore volume (V_{total}) of the Z5-0.18 sample slightly decreased compared with the Z5-0 sample, which may be brought by the larger size of the crystals synthesized in the urea-containing medium.

It has been reported that the surface Si-zoned ZSM-5 with a siliceous exterior could promote shape selectivity due to the decrease of acid sites on the external surface, where a non-

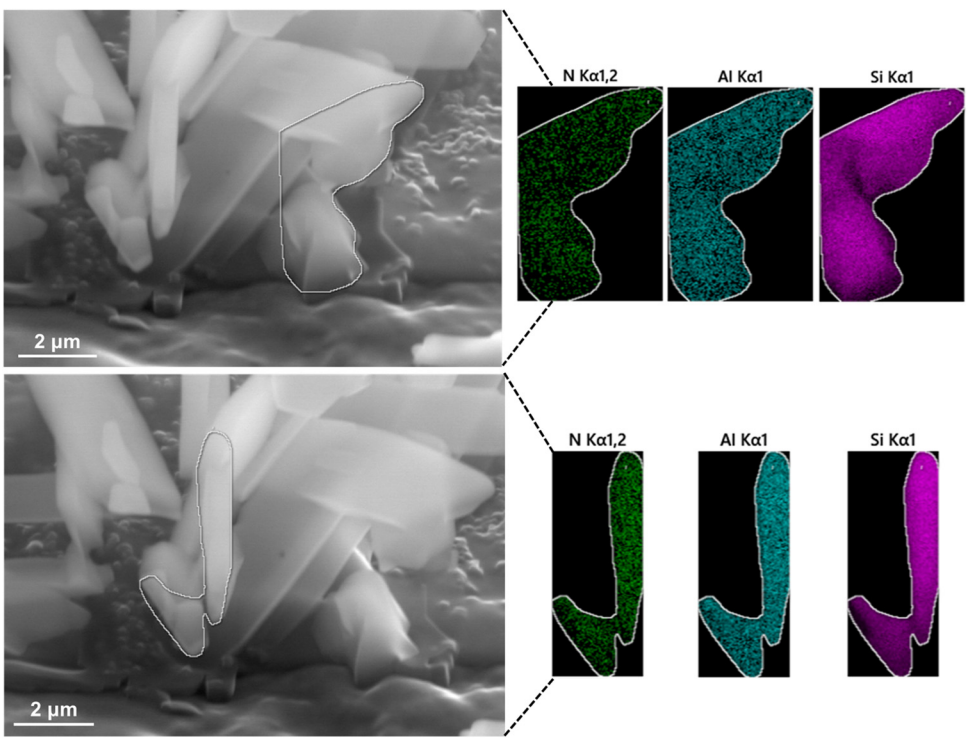

Fig. 3 Cross-section cuts of Z5-0.18 catalysts along the *b*-axis orientation (two cutting positions, marked with a white circle) constructed by FIB, and the corresponding EDS mapping images of Z5-0.18 are displayed on the right: N (green), Al (blue), and Si (pink).

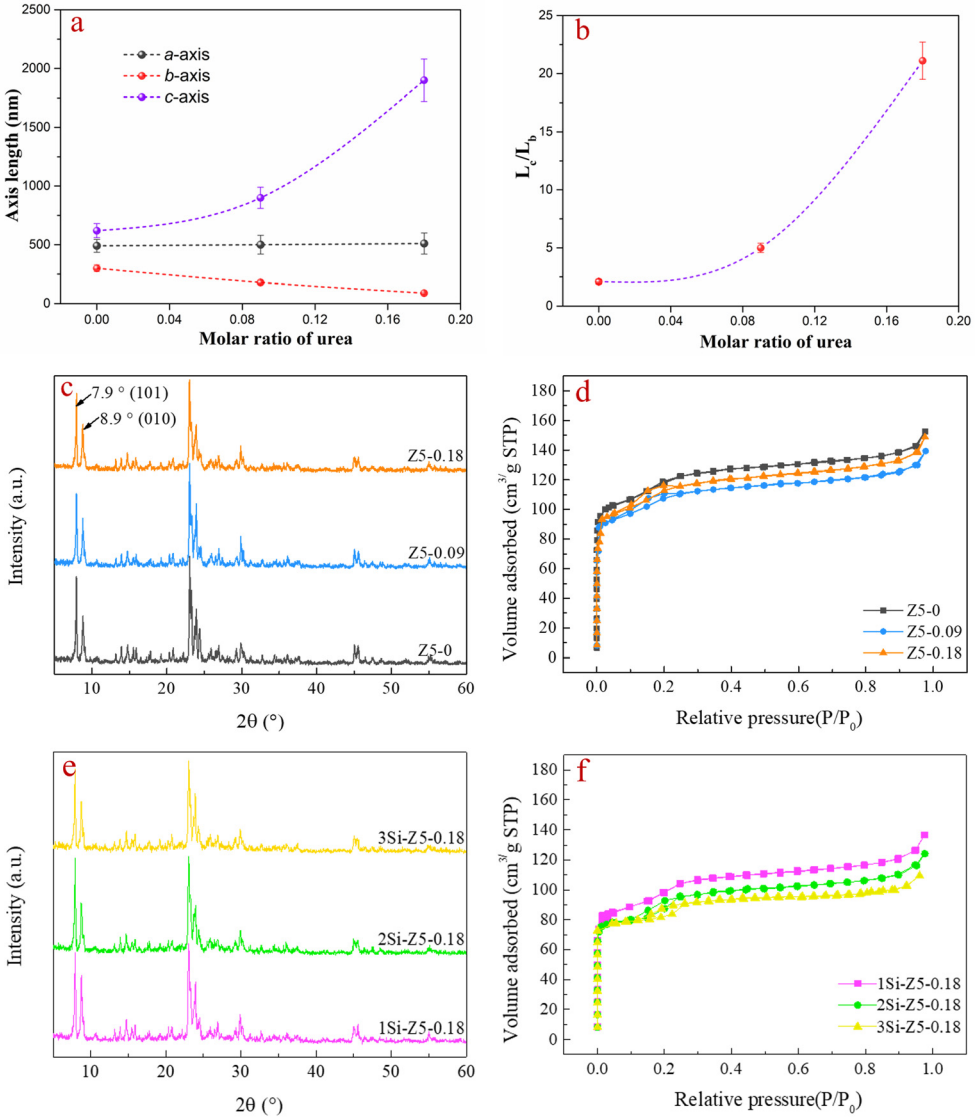

Fig. 4 (a) The length along the three axes and (b) L_c/L_b aspect ratios of ZSM-5 with different *b*-axis thicknesses. (c) XRD patterns and (d) N_2 adsorption–desorption isotherms of ZSM-5 with different *b*-axis thicknesses. (e) XRD patterns and (f) N_2 adsorption–desorption isotherms of platelike ZSM-5 after different SiO_2-CLD modification times.

Table 1 Textural properties of ZSM-5 with different *b*-axis thicknesses

		Average axis length[b] (nm)			Specific surface area[c] ($m^2\ g^{-1}$)			Pore volume[d] ($cm^3\ g^{-1}$)		
Sample	Si/Al[a]	*a*	*b*	*c*	S_{BET}	S_{micro}	S_{ext}	V_{total}	V_{micro}	V_{meso}
Z5-0	53.7	490	300	620	414	363	51	0.236	0.173	0.092
Z5-0.09	54.4	500	180	900	403	358	45	0.230	0.169	0.095
Z5-0.18	52.9	510	90	1900	391	355	36	0.225	0.167	0.088

[a] Determined by the XRF results. [b] Determined by statistics of 100 specimens in SEM images displayed in Fig. 1. [c] Calculated by the BET method and *t*-plot method. [d] Calculated by the *t*-plot method.

shape-selective catalytic process occurs.[34–36] Thus, the SiO_2 surface modified ZSM-5 catalysts were prepared by a chemical liquid phase deposition (CLD) method, and the yield of ZSM-5 zeolite products after each cycle of SiO_2 modification, as shown in Table S1.† Detailed synthesis conditions are reported in the Experimental section. In the XRD results, all SiO_2 modified samples exhibit typical characteristic peaks of the MFI phase with a sound crystallinity (Fig. 4e). Meanwhile, all SiO_2

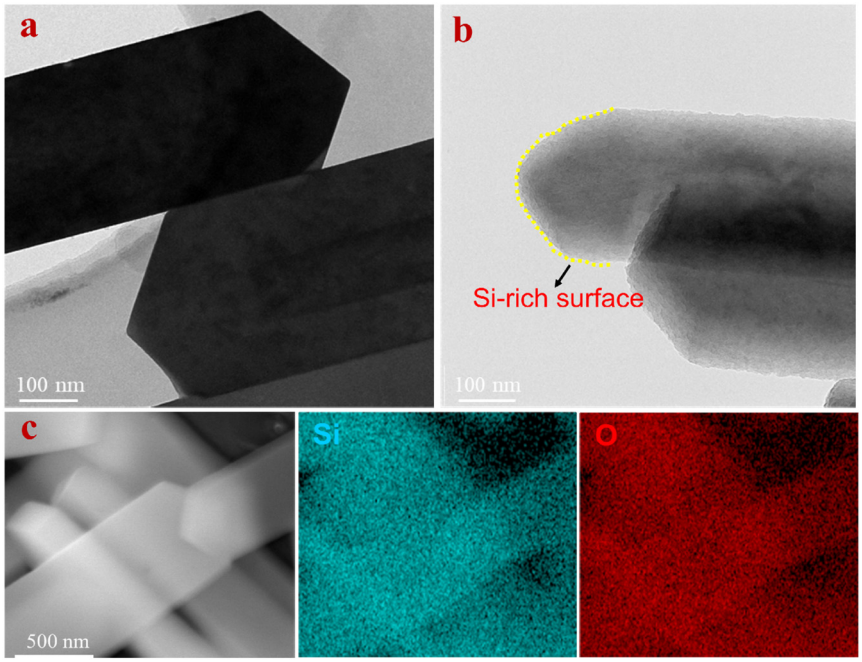

Fig. 5 TEM images of (a) Z5-0.18, (b) 3Si-Z5-0.18 samples and (c) the SEM-EDS mapping images of 3Si-Z5-0.18.

modified samples show type-I isotherms with fast uptake at low relative pressure in the N_2 adsorption–desorption isotherms, which is similar to those of ZSM-5 before SiO_2 modification (Fig. 4f). These results imply that the CLD modification does not damage the zeolite framework and the inherent microporous structure. In addition, the BET surface area (S_{BET}) gradually declined from 1Si-Z5-0.18 to 3Si-Z5-0.18 (Table S2†), caused by the intensive Si coating. Notably, the 3Si-Z5-0.18 sample after 3 times SiO_2-CLD modification shows a distinct siliceous shell compared to that of the parent Z5-0.18 sample, as shown in Fig. 5a and b. Furthermore, the SEM-EDS elemental mapping images are shown in Fig. 5c. Evidently, the abundant Si elements in the 3Si-Z5-0.18 sample intuitively demonstrate the Si-rich surface of 3Si-Z5-0.18, which is in good agreement with the TEM results.

3.2 Acid properties

To establish the structure–property relationship, the acidity of ZSM-5 catalysts with different *b*-axis thicknesses is investigated by means of NH_3-TPD and Py-IR. As shown in Fig. 6a, all the samples show two distinct NH_3 desorption peaks, inferring the existence of two kinds of acid sites on these catalysts. The desorption peak at temperatures lower than 300 °C was associated with weakly acidic silanol groups and weak Lewis (or Brønsted) acid sites, while the other peak ranging from 300 to 600 °C was associated with stronger acid sites.[29] The concentrations of total acid sites are nearly identical in these samples due to their similar Si/Al ratios (Table 1). Notably, the strength of weak acid slightly increased from Z5-0 to Z5-0.18, whereas the strength of strong acid diminished to some extent. These minor differences between the ZSM-5 with different *b*-axis thicknesses suggest that the partial nature of acid and base sites may be changed from Z5-0 to Z5-0.18.

Then, the FTIR spectra using pyridines (Py) as probe molecules are recorded for gaining a deeper understanding of the nature of acid sites. The bands at 1455 cm^{-1} could be ascribed to pyridines–Lewis acid site (LAS) interaction, while the band at around 1545 cm^{-1} could be assigned to pyridines–Brønsted acid site (BAS) interaction.[30] As shown in Fig. 6b, the concentration of LASs mildly increased from Z5-0 to Z5-0.18 at the evacuation temperature of both 100 °C and 300 °C, while the BAS concentrations among these catalysts are nearly the same. Moreover, the LASs/BASs ratios (*L*/*B*) were obviously increased as the *b*-axis thickness became smaller. For example, the *L*/*B* ratios were 0.45 and 0.07 for Z5-0.18 and Z5-0 at 300 °C, respectively (Table 2). We reasonably suppose that the difference in acidic nature among these catalysts might be attributed to the introduction of N species over the Z5-0.18 catalyst, which is in agreement with our previous work.[31] Additionally, solid-state MAS ^{27}Al spectra are used to investigate the local Al coordination environments of these catalysts, which are closely related to Lewis acid–base sites. As shown in Fig. 7, all samples show one dominant peak at around 52–57 ppm, which can be attributed to tetrahedral Al species. A new weak peak at ~0 ppm is observed for Z5-0.09 and Z5-0.18 catalysts, assigned to octahedral Al (*i.e.*, extra-framework species acting as surface LASs). It seems that the transformation of tetrahedral Al to octahedral Al implies the reconstruction of surface Lewis acid sites on the platelike zeolites.

On the other hand, the acid properties of Z5-0.18 samples after 1–3 times SiO_2-CLD modification were further investigated. NH_3-TPD results show that both the weak and strong

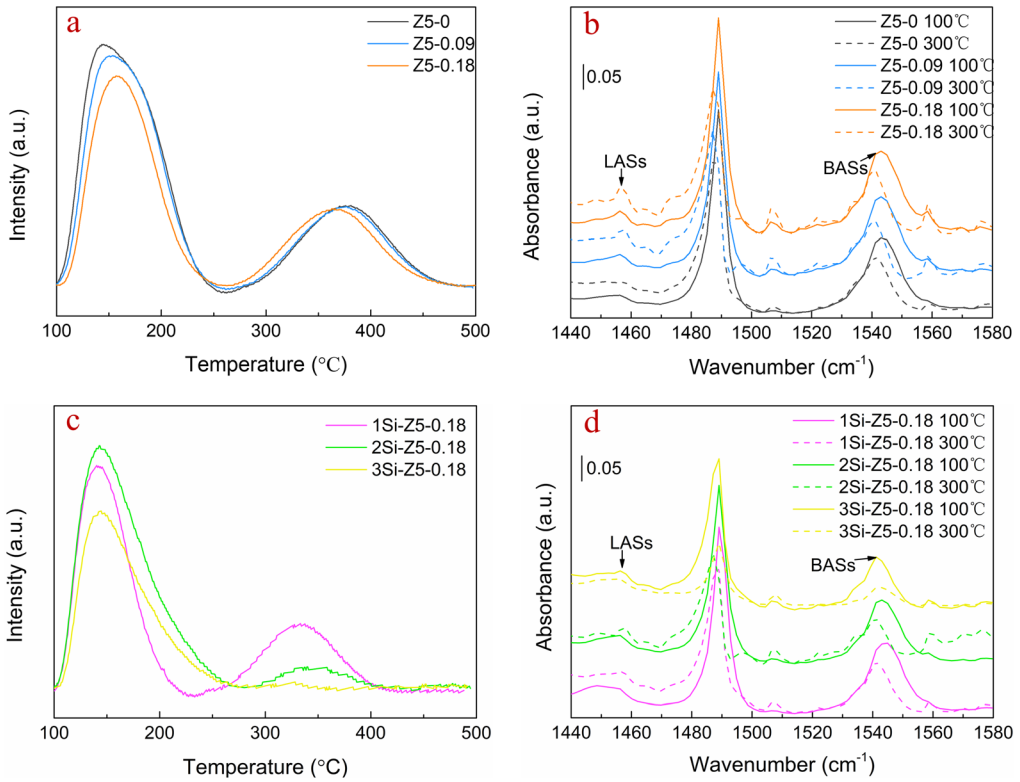

Fig. 6 The characterization of acid properties of platelike ZSM-5 samples before and after SiO_2-CLD modification. (a) NH_3-TPD profiles and (b) Py adsorbed FTIR spectra of the platelike ZSM-5 samples before SiO_2 modification. (c) NH_3-TPD profiles and (d) Py adsorbed FTIR spectra of platelike ZSM-5 after different SiO_2-CLD modification times.

Table 2 Acid properties of the platelike ZSM-5 samples before and after SiO_2-CLD modification

	Acidity determined by NH_3-TPD (mmol g^{-1})			Acidity determined by Py-IR	
Samples	Total	Weak	Strong	*L*/*B* (100 °C)	*L*/*B* (300 °C)
Z5-0	0.33	0.21	0.12	0.15	0.07
Z5-0.09	0.31	0.20	0.11	0.25	0.21
Z5-0.18	0.29	0.18	0.11	0.27	0.45
1Si-Z5-0.18	0.22	0.13	0.09	0.26	0.11
2Si-Z5-0.18	0.20	0.17	0.03	0.17	0.14
3Si-Z5-0.18	0.14	0.13	0.01	0.13	—

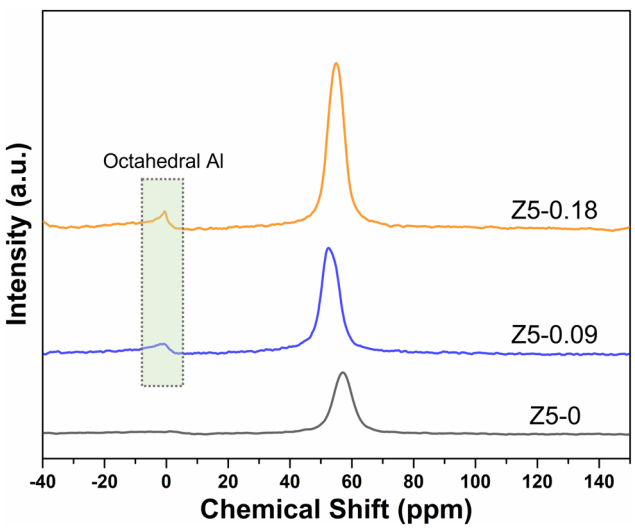

Fig. 7 Solid-state^{27} Al MAS NMR spectra of Z5-0, Z5-0.09 and Z5-0.18 catalysts.

acid sites decreased with increasing SiO_2 modification times (Fig. 6c). In particular, for 3Si-Z5-0.18, the NH_3 desorption peak representing strong acid sites (>300 °C) even disappeared. This might be attributed to the weakening or even absence of external acidity of Z5-0.18 *via* SiO_2-CLD surface modification. Moreover, the Py-IR results indicate that both the concentration of BASs and LASs decreased in the order of 1Si-Z5-0.18 > 2Si-Z5-0.18 > 3Si-Z5-0.18 after desorption at 100 °C (Fig. 6d). The number of acid sites on these prepared *y*Si-Z5-0.18 catalysts are summarized in Table 2 and Table S3.† The 3Si-Z5-0.18 sample shows a smaller number of BASs (0.08 mmol g^{-1}) compared to the parent Z5-0.18 of 0.17 mmol g^{-1}, 1Si-Z5-0.18 of 0.15 mmol g^{-1} and 2Si-Z5-0.18 of 0.12 mmol g^{-1}. Meanwhile, the amount of LASs in 3Si-Z5-0.18 of 0.01 mmol g^{-1} is also lower than that of parent Z5-0.18, 1Si-Z5-0.18 and 2Si-Z5-0.18. In addition, as the evacuation temperature increases, the intensity of all peaks decreases obviously at 300 °C, and almost disappears for the 3Si-Z5-0.18 sample (dashed line in

Fig. 6d). This result matches well with the NH_3-TPD results in Fig. 6c, implying the predominant presence of weak acid sites in 3Si-Z5-0.18. Differently, the parent Z5-0.18 has much more strong BASs than 3Si-Z5-0.18 (0.11 mmol g^{-1} *vs.* 0.02 mmol g^{-1}).

The catalytic cracking of bulky triisopropylbenzene (TIPB) is an effective method to evaluate the external surface acidic properties of ZSM-5 since TIPB has a kinetic diameter of 0.85 nm and will not enter the ZSM-5 pores.[37–39] Fig. S1† shows a dramatic reduction in the TIPB conversion from parent Z5-0.18 to 3Si-Z5-0.18 (40.2% *vs.* 5.2%), implying that 3Si-Z5-0.18 features less external surface acid sites. This can be attributed to the fact that 3Si-Z5-0.18 exhibits a Si-rich surface compared to that of parent Z5-0.18.

3.3 Catalytic performance

The reaction of toluene alkylation with ethanol is conducted over ZSM-5 samples with different *b*-axis thicknesses, aiming to gain insight into the intrinsic effect of *b*-axis lengths on the catalytic performance. Toluene conversion, ethyltoluene (ET) selectivity and *para*-ethyltoluene (*p*-ET) selectivity as a function of time are shown in Fig. 8a–c, respectively. It seems that differences in catalytic activity are obvious over these three catalysts. As the *b*-axis thickness decreases, an inspiring catalytic behavior is observed, involving the gradual increase of toluene conversion and ethyltoluene selectivity. Typically, the Z5-0.18 catalyst showed superior catalytic performance in comparison with the Z5-0 catalyst, in terms of toluene conversion (58.3% *vs.* 37.8%) and ethyltoluene selectivity (88.7% *vs.* 57.1%) under identical reaction conditions (400 °C, TOS = 8 h). Meanwhile, the reaction results at TOS of 8 h are summarized in more detail in Table 3 and Fig. S2.† Clearly, ET is the primary product over all the samples, whereas benzene, xylene and other C_9^+ aromatics are major by-products. Besides, the distribution of gaseous products is provided in Table S4.† It is evident that C_2H_4 is the primary gaseous product, and other gaseous products including CH_4, C_2H_6, C_3H_6 as well as C_4-C_5 are also detected.

The variations in catalytic performance can be attributed to the different structural and acidic properties of these zeolite catalysts. First, the conceivable introduction of N species into platelike ZSM-5, which modulates the Lewis acid sites (as confirmed by the results in Fig. 6 and Table 2), should be one of the reasons for the superior activity of the Z5-0.18 catalyst. More importantly, the large aromatic molecules preferentially diffuse through the straight channels rather than sinusoidal channels, as proposed by previous studies.[32,33] That is to say, the difference in the lengths of ZSM-5 along the *b*-axes and *c*-axes could alter the diffusion rates of guest molecules, thereby affecting catalytic performances. For example, the much higher L_c/L_b aspect ratios of Z5-0.18 (21.2) compared to Z5-0 (2.1) would contribute to enhanced mass transfer, thus improving the accessibility of active sites and toluene conversion. Moreover, the shortened *b*-axes could hinder the enrichment of ethanol molecules, which benefits from the utilization of ethanol in alkylation, thereby leading to a higher ET selectivity on Z5-0.18.

We monitor the quantity of coke species during the alkylation reaction by using TG analysis. As shown in Fig. S3,† the weight loss due to carbon combustion and decomposition on the spent Z5-0.18 catalyst after the reaction is lower than spent Z5-0.09 and Z5-0 catalysts (Fig. S3a†). Meanwhile, the calculated amount of coke deposited on spent Z5-0.18 is 8.1 mg_{coke} $g_{catalyst}^{-1}$ (Fig. S3b†), which is also lower than the spent Z5-0.09 (17.4) and

Table 3 Catalytic performances over different ZSM-5 zeolites for the reaction of toluene alkylation with ethanol

Sample		Z5-0	Z5-0.09	Z5-0.18
Products distribution[a] (%)	Non-aromatic	0.96	1.03	0.78
	Benzene	2.91	1.17	0.44
	Toluene	62.20	50.82	41.72
	Ethylbenzene	2.32	2.03	1.37
	Xylene	5.80	4.02	1.74
	p-ET	5.79	10.94	15.56
	m-ET	12.78	23.76	35.63
	o-ET	3.00	2.81	0.52
	Others	4.24	3.42	2.24
Calculated data (%)	C_T (%)	37.8	49.2	58.3
	S_{ET} (%)	57.1	76.2	88.7
	$S_{p\text{-}ET}$ (%)	27.1	29.4	29.8

Reaction conditions: 400 °C, toluene/ethanol ratio = 1.0, WHSV = 2.0 h^{-1}. [a] Determined at 8 h time-on-stream.

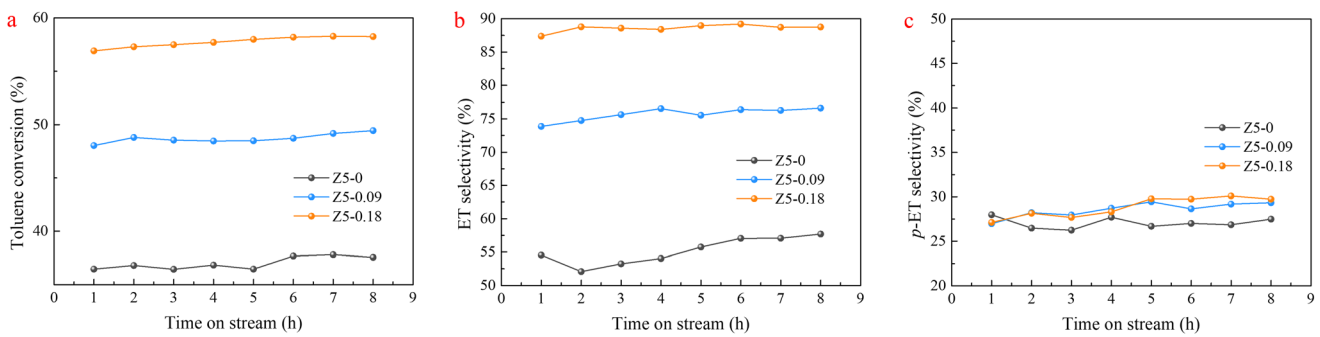

Fig. 8 Catalytic performance of ZSM-5 catalysts with different lengths of the *b*-axis. (a) Toluene conversion. (b) Selectivity of ethyltoluene. (c) Selectivity of *para*-ethyltoluene. Reaction conditions: 400 °C, toluene/ethanol ratio = 1.0, WHSV = 2.0 h^{-1}.

spent Z5-0 (30.7), indicating the superior anti-carbon deposition ability of Z5-0.18. This may also be attributed to the shortened *b*-axis and fast diffusion of our platelike structure, thus suppressing the formation of coke precursors such as ethylene and large polycyclic aromatic hydrocarbons. It is worth noting that the shortened *b*-axis of Z5-0.18 seems to have no significant positive impact on *para*-selectivity, as the *p*-ET selectivity on all three catalysts remains at thermodynamic equilibrium levels, approximately 27% to 30% (Fig. 8c). The shape-selective capability of the platelike ZSM-5 zeolite still needs to be further exploited.

Therefore, the catalytic performance for the alkylation of toluene with ethanol over the silicate-passivated ZSM-5 catalyst are investigated to verify the effect of the Si-rich external surface on ZSM-5's shape-selective capability. As listed in Table 4, ET is the primary product over all the catalysts, whereas benzene, xylene, ethylbenzene, non-aromatic and other C_9^+ aromatics are major byproducts. This product distribution aligns with that of the parent Z5-0.18 catalyst. To our delight, with the increase of SiO_2-CLD modification times, the selectivity of *para*-ethyltoluene gradually increased while the total ethyltoluene selectivity among these three catalysts showed no obvious change (Fig. 9b and c). Notably, the 3Si-Z5-0.18 catalyst exhibited significantly better shape-selective performance in comparison with the parent Z5-0.18 catalyst, in terms of *para*-ethyltoluene selectivity (96.2% *vs.* 29.8%, TOS = 8 h), as well as other catalysts reported in the literature (Table S5†). The alkylation performance of toluene with ethanol over different catalysts in the literature was studied. Nevertheless, the toluene conversion gradually decreased with the increasing Si modification times (Fig. 9a). The primary reason, for the higher toluene conversion of parent Z5-0.18 than the silicate-passivated ZSM-5 (*ex.*, 3Si-Z5-0.18), a prevailing view is the occurrence of non-shape-selective reactions over

Table 4 The summary of toluene alkylation with ethanol over the prepared *y*Si-Z5-0.18 catalysts

Sample		1Si-Z5-0.18	2Si-Z5-0.18	3Si-Z5-0.18
Product distribution[a] (%)	Non-aromatic	0.42	0.16	0.08
	Benzene	0.64	0.59	0.21
	Toluene	52.34	64.81	82.07
	Ethylbenzene	0.54	0.51	0.39
	Xylene	1.68	1.18	0.81
	p-ET	21.06	26.99	15.27
	m-ET	20.66	4.03	0.51
	o-ET	1.27	0.68	0.09
	Others	1.39	1.05	0.57
Calculated data	C_T (%)	47.6	35.19	17.9
	S_{ET} (%)	90.3	90.1	88.7
	$S_{p\text{-}ET}$ (%)	49.0	85.1	96.2

Reaction conditions: 400 °C, toluene/ethanol ratio = 1.0, WHSV = 2.0 h^{-1}. [a] Determined at 8 h time-on-stream.

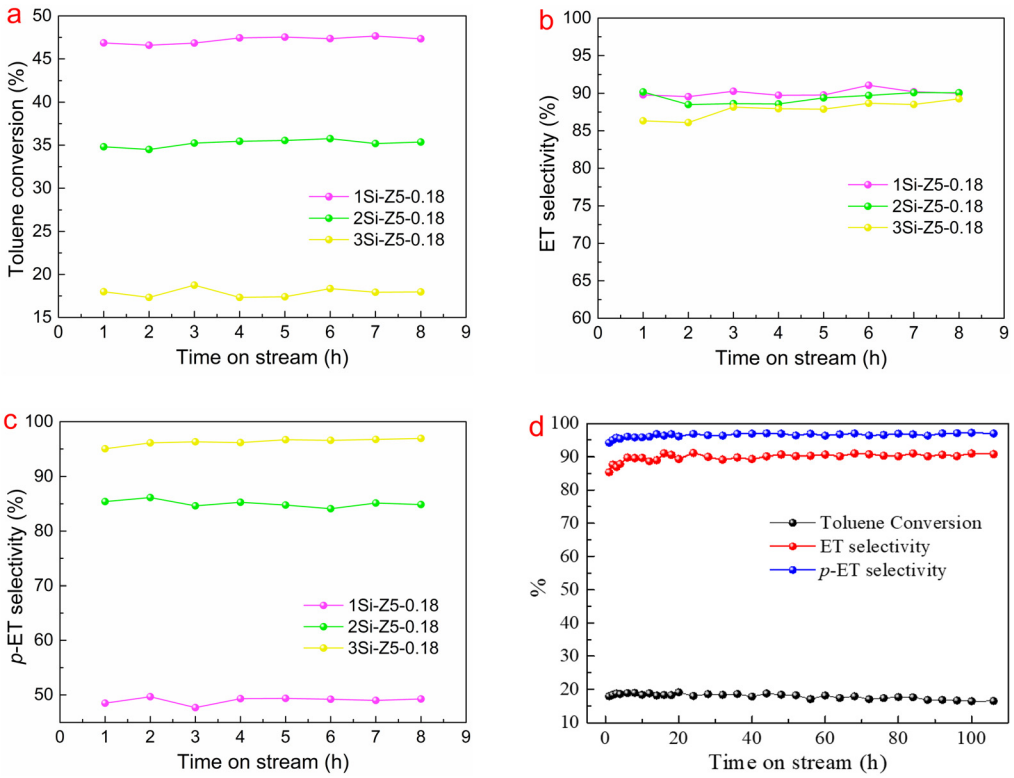

Fig. 9 Catalytic performance of platelike ZSM-5 with different SiO_2-CLD modification times. (a) Toluene conversion. (b) Selectivity of ethyltoluene. (c) Selectivity of *para*-ethyltoluene. (d) Catalytic stability test for the reaction of toluene alkylation with ethanol over the 3Si-Z5-0.18 catalyst (>100 h). Reaction conditions: 400 °C, toluene/ethanol ratio = 1.0, WHSV = 2.0 h^{-1}.

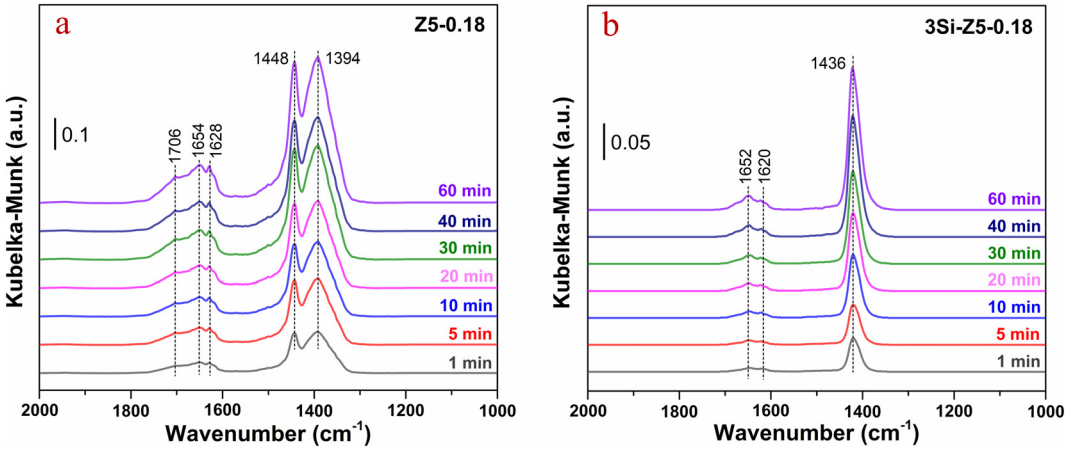

Fig. 10 Time-dependent *in situ* DRIFTS during the alkylation reaction on (a) Z5-0.18 and (b) 3Si-Z5-0.18. The spectra were collected from 1 min to 60 min at 400 °C.

the crystals' external acid sites of parent Z5-0.18.[40,41] Another observation is the excellent catalytic stability of the 3Si-Z5-0.18 catalyst in the long-time test. As shown in Fig. 9d, the toluene conversion, ET selectivity and *p*-ET selectivity of 3Si-Z5-0.18 exhibit almost no drop after 100 h reaction, indicating a better potential for practical applications.

In addition, the time-dependent *in situ* DRIFTS studies are performed to gain insights into the variation of organic species reaction intermediates on the surface of the platelike ZSM-5 before and after 3 times SiO_2-CLD modification (Z5-0.18 *vs.* 3Si-Z5-0.18) for the alkylation of toluene with ethanol at 400 °C (Fig. 10). For both Z5-0.18 and 3Si-Z5-0.18 catalysts under study, the peaks at around 1448, 1628 and 1654 cm^{-1} are observed, which are assigned to the C–H stretching vibrations, skeletal C=C vibrations of aromatics and bending vibrations of the C–H bond.[42] These peaks observed for Z5-0.18 are significantly stronger than those of 3Si-Z5-0.18, implying the relatively retarded desorption of hydrocarbons from the Z5-0.18 due to its stronger BASs than 3Si-Z5-0.18, thereby making it more susceptible to further isomerization leading to a low p-ET selectivity and deep alkylation leading to heavy aromatics. Furthermore, the Z5-0.18 catalyst exhibits another two peaks at 1394 and 1706 cm^{-1}. These peaks are indicative of C–H stretching vibrations that are characteristic of carbon atoms with double bonds, such as olefins and dienes.[38] However, these peaks are not observed in the 3Si-Z5-0.18 catalyst. Previous studies have reported that the polymerization of olefins is more likely to occur on BASs; thus, the accumulation of light olefins within the pores of Z5-0.18 may accelerate the formation of oligomerization species (*ex.*, coke-inducing aromatics), leading to the deactivation of the catalyst.[43]

4 Conclusion

In summary, the *b*-axis-oriented ZSM-5 catalysts with different thicknesses (90, 180, and 300 nm) are successfully prepared *via* a urea-assisted crystallization strategy. Subsequently, the performances of these ZSM-5 catalysts in the toluene alkylation reaction with ethanol are investigated. Among them, the thinnest Z5-0.18 catalyst exhibited both higher toluene conversion (58.3%) and styrene selectivity (88.7%). This is primarily ascribed to the shortened straight channels of plate-like ZSM-5, which facilitate mass transport and increase the accessibility to acid sites. Meanwhile, the unexpected N doping seems to modulate the surface Lewis acid sites on Z5-0.18 due to its ability to donate electrons. Moreover, we constructed a Si-zoned external surface on the plate-like ZSM-5 by means of the surface modification strategy to accurately passivate the surface acid sites, thereby inhibiting the isomerization reaction, and achieving higher selectivity for *p*-ET (>95%), accompanied by extended catalytic stability (>100 h) in the reaction of toluene alkylation with ethanol. We posit that this fundamental work could provide new opportunities for the design of highly efficient catalysts for toluene alkylation with ethanol and other catalytic reactions controlled by acid sites and diffusion, synergistically. It is reasonable to believe that the *b*-axis oriented platelike zeolites are promising candidates for further industrial applications.

Data availability

All data needed to support the findings of this study are included in the main text or in the ESI.† Any additional information may be available from the corresponding authors upon request.

Conflicts of interest

There are no conflicts to declare.

Acknowledgements

The work described above was supported by the National Natural Science Foundation of China (91534115), the Zhejiang Provincial Natural Science Foundation of China (ZCLQN25B0303), the General Research Project of Zhejiang Provincial Department of Education (Y202352170) and Jiaxing City Public Welfare Research Project of China (2024AY10024). The authors gratefully acknowledge the support from the Guangzhou Institute for Food Inspection (Doctoral Workstation of Guangdong Province). The authors also extend their gratitude to the researchers from Shiyanjia Lab (**https://www.shiyanjia.com**) for their help with AFM and FIB-SEM analyses.

References

1 W. Kaeding, Shape-selective reactions with zeolite catalysts: IV. Alkylation of toluene with ethylene to produce p-ethyltoluene, *J. Catal.*, 1984, **89**(2), 267–273.
2 S. Al-Khattaf, S. A. Ali, A. M. Aitani, N. Žilková, D. Kubička and J. Čejka, Recent Advances in Reactions of Alkylbenzenes Over Novel Zeolites: The Effects of Zeolite Structure and Morphology, *Catal. Rev.*, 2014, **56**(4), 333–402.
3 J. Walendziewski and J. Trawczyński, Alkylation of Toluene with Ethanol, *Ind. Eng. Chem. Res.*, 1996, **35**(10), 3356–3361.
4 B. Ogunbadejo, A. Aitani, J. Cejka, M. Kubu and S. Al-Khattaf, The effect of alkylation route on ethyltoluene production over different structural types of zeolites, *Chem. Eng. J.*, 2016, **306**, 1071–1080.
5 B. A. Ogunbadejo, M. S. Osman, P. Arudra, A. M. Aitani and S. S. Al-Khattaf, Alkylation of toluene with ethanol to para-ethyltoluene over MFI zeolites: Comparative study and kinetic modeling, *Catal. Today*, 2015, **243**, 109–117.
6 K. Ithisuphalap, M. A. Nolen, H. Monroe and S. Kwon, Kinetic, Spectroscopic, and Theoretical Study of Toluene Alkylation with Ethylene on Acidic Mordenite Zeolite, *ACS Catal.*, 2023, **13**(24), 16012–16031.
7 Z. Hong, C. F. Xiong, X. Wang, F. T. Huang, L. Li and Z. R. Zhu, Ammonia pools effect in Cs modified X zeolites for side-chain alkylation of toluene with methanol, *Chem. Eng. J.*, 2023, **474**, 145650.
8 C. S. Lee, T. J. Park and W. Young, Alkylation of toluene over double structure ZSM-5 type catalysts covered with a silicalite shell, *Appl. Catal., A*, 1993, **96**(2), 151–161.
9 M. Niwa, M. Kato, T. Hattori and Y. Murakami, Fine control of the pore-opening size of zeolite ZSM-5 by chemical vapor deposition of silicon methoxide, *J. Phys. Chem.*, 1984, **11**, 1–11.
10 Z. Hong, C. F. Xiong, G. Q. Zhao and Z. R. Zhu, Side-chain alkylation of toluene with methanol to produce styrene: an overview, *Catal. Sci. Technol.*, 2019, **9**(24), 6828–6840.
11 X. Liu, J. Shi, G. Yang, J. Zhou, C. Wang, J. Teng, Y. Wang and Z. Xie, A diffusion anisotropy descriptor links morphology effects of H-ZSM-5 zeolites to their catalytic cracking performance, *Commun. Chem.*, 2021, **4**, 107–117.
12 X. Huang, R. Wang, X. Pan, C. Wang and J. Peng, Catalyst Design Strategies towards Highly Shape-selective HZSM-5 for Para-xylene through Toluene Alkylation, *Green Energy Environ.*, 2020, **5**(4), 385–393.
13 H. Hu, J. Lyu, Q. Wang, Q. Zhang, J. Cen and X. Li, Alkylation of benzene with methanol over hierarchical porous ZSM-5: synergy effects of hydrogen atmosphere and zinc modification†, *RSC Adv.*, 2015, **5**(41), 32679–32684.
14 J.-H. Lyu, H.-L. Hu, J.-Y. Rui, Q.-F. Zhang, J. Cen, W.-W. Han, Q.-T. Wang, X.-K. Chen, Z.-Y. Pan and X.-N. Li, Nitridation: A simple way to improve the catalytic performance of hierarchical porous ZSM-5 in benzene alkylation with methanol, *Chin. Chem. Lett.*, 2017, **28**(2), 482–486.
15 M. Choi, K. Na, J. Kim, Y. Sakamoto, O. Terasaki and R. Ryoo, Stable single-unit-cell nanosheets of zeolite MFI as active and long-lived catalysts, *Nature*, 2009, **461**(7261), 246–249.
16 W. J. Dai, C. Kouvatas, W. S. Tai, G. J. Wu, N. J. Guan, L. D. Li and V. Valtchev, Platelike MFI Crystals with Controlled Crystal Faces Aspect Ratio, *J. Am. Chem. Soc.*, 2021, **143**(4), 1993–2004.
17 Y. Sun, S. W. Cao, J. Wang, H. Tang, Z. K. Yang, T. Ma, Y. J. Gong, G. Mo and Z. H. Li, Fabrication of Twin-Free Nanoslab ZSM-5 Zeolite with b-Axis Orientation for Super MTP Catalyst, *ACS Sustainable Chem. Eng.*, 2022, **10**(29), 9431–9442.
18 Z. Jiaxing, Z. Ajuan, G. Kaivalya, L. Guanxing, S. Shujie, D. Chengyi, F. Wei, H. Yu, S. Chunshan, R. Limin, Z. Anfeng and G. Xinwen, b-Axis-Oriented ZSM-5 Nanosheets for Efficient Alkylation of Benzene with Methanol: Synergy of Acid Sites and Diffusion, *ACS Catal.*, 2023, **13**, 3794–3805.
19 A. J. Zhou, J. X. Zhang, H. Yang, S. J. Shang, A. F. Zhang, C. S. Song and X. W. Guo, Synergetic and efficient alkylation of benzene with ethane over Pt/ZSM-5 nanosheet bifunctional catalysts to ethylbenzene, *Fuel*, 2023, **342**, 127764.
20 J. X. Zhang, L. M. Ren, A. J. Zhou, W. H. Li, S. J. Shang, Y. Liu, Z. H. Jia, W. Liu, A. F. Zhang, X. W. Guo and C. S. Song, Tailored Synthesis of ZSM-5 Nanosheets with Controllable b-Axis Thickness and Aspect Ratio: Strategy and Growth Mechanism, *Chem. Mater.*, 2022, **34**(7), 3217–3226.
21 H. Li, J. Y. Yu, K. Du, W. Y. Li, L. Ding, W. Chen, S. H. Xie, Y. H. Zhang and Y. Tang, Synthesis of ZSM-5 Zeolite Nanosheets with Tunable Silanol Nest Contents across an Ultra-wide pH Range and Their Catalytic Validation, *Angew. Chem., Int. Ed.*, 2024, **63**(24), e202405092.
22 L. H. Guo, Y. J. Tian, X. Y. He, C. Z. Qiao and G. Z. Liu, Hydrodeoxygenation of phenolics over uniformly dispersed Pt-Ni alloys supported by self-pillared ZSM-5 nanosheets, *Fuel*, 2022, **322**, 124082.

23 J. Kärger and D. M. Ruthven, Diffusion in nanoporous materials: fundamental principles, insights and challenges, *New J. Chem.*, 2016, **40**(5), 4027–4048.
24 Z. Hong, L. Li, L. Miao, G. Q. Zhao and Z. R. Zhu, Opening sodalite cages of X zeolite for boosting toluene side-chain alkylation performance, *Catal. Sci. Technol.*, 2023, **13**(7), 1991–1995.
25 J. Zhang, W. Qian, C. Kong and F. Wei, Increasing para-Xylene Selectivity in Making Aromatics from Methanol with a Surface-Modified Zn/P/ZSM-5 Catalyst, *ACS Catal.*, 2015, **5**(5), 2982–2988.
26 Z. Shan, H. Wang, X. Meng, S. Liu, L. Wang, C. Wang, F. Li, J. P. Lewis and F.-S. Xiao, Designed synthesis of TS-1 crystals with controllable b-oriented length, *Chem. Commun.*, 2011, **47**(3), 1048–1050.
27 J. Yang, K. Gong, D. Miao, F. Jiao, X. Pan, X. Meng, F. Xiao and X. Bao, Enhanced aromatic selectivity by the sheet-like ZSM-5 in syngas conversion, *J. Energy Chem.*, 2018, **35**, 44–48.
28 Y. Liu, X. Zhou, X. Pang, Y. Jin, X. Meng, X. Zheng, X. Gao and F.-S. Xiao, Improved para–Xylene Selectivity in meta–Xylene Isomerization Over ZSM–5 Crystals with Relatively Long b–Axis Length, *ChemCatChem*, 2013, **5**(6), 1517–1523.
29 Z. Hong, Z. Wang, D. Chen, Q. Sun and X. Li, Hollow ZSM-5 encapsulated Pt nanoparticles for selective catalytic reduction of NO by hydrogen, *Appl. Surf. Sci.*, 2018, **440**, 1037–1046.
30 H. Q. Wang, B. Y. Shen, X. Chen, H. Xiong, H. M. Wang, W. L. Song, C. J. Cui, F. Wei and W. Z. Qian, Modulating inherent lewis acidity at the intergrowth interface of mortise-tenon zeolite catalyst, *Nat. Commun.*, 2022, **13**(1), 2924–2933.
31 Z. Hong, X. Wang, Y. S. Fang, L. H. Deng, L. Li and Z. R. Zhu, Restructuring Surface Lewis Pairs of FAU Zeolite through N Doping for Boosting the Toluene Side-Chain Alkylation Performance, *Inorg. Chem.*, 2024, **63**(7), 3258–3266.
32 N. Wang, W. Sun, Y. Hou, B. Ge, L. Hu, J. Nie, W. Qian and F. Wei, Crystal-plane effects of MFI zeolite in catalytic conversion of methanol to hydrocarbons, *J. Catal.*, 2018, **360**, 89–96.
33 Z. Yan, D. Chen, L. Huang, J. Liu, H. Fu, Y. Xiao and S. Li, A theoretical insight into diffusion mechanism of benzene-methanol alkylation reaction in ZSM-5 zeolite, *Microporous Mesoporous Mater.*, 2022, **337**, 111926.
34 F. Jiao, P. Y. Yu, Y. C. Cui, H. Li, Q. Hu, Y. A. Xu, S. Mintova, H. L. Guo and H. B. Du, Hollow STW-Type Zeolite Single Crystals with Aluminum Gradient for Highly Selective Production of p-Xylene from Methanol-Toluene Alkylation, *Angew. Chem., Int. Ed.*, 2023, **62**(41), e202310419.
35 Z. Hong, L. Deng, F. Wang, F. Zhu, Y. Fang, L. Song, L. Li and Z. Zhu, Intergrowth MFI Zeolite with Inverse Al Zoning and Predominant Sinusoidal Channels for Highly Selective Production of Styrene, *Inorg. Chem.*, 2024, **63**(43), 20888–20899.
36 J. Q. Hao, J. Zhou, Y. D. Wang, L. Y. Li, Z. Z. Sheng, J. W. Teng and Z. K. Xie, Pore mouth catalysis promoting n-hexane hydroisomerization over a Pt/ZSM-5 bifunctional catalyst, *Chem Catal.*, 2024, **4**(8), 101041.
37 Z. Hong, G. Q. Zhao, C. F. Xiong, W. Z. Jia, F. T. Huang and Z. R. Zhu, Cesium-modified hollow ZSM-5: Efficient acid-base catalyst for side-chain alkylation of 2-picoline with formaldehyde, *Appl. Catal., A*, 2021, **612**, 117983.
38 F. T. Huang, Z. Hong, L. Li, L. Miao, X. L. Gao, G. Q. Zhao and Z. R. Zhu, Shape-Selective Alkylation of Toluene with Ethanol over a Twin Intergrowth Structured ZSM-5: Modulation of Acidity and Diffusivity via Interface Engineering, *Inorg. Chem.*, 2024, **63**(7), 3506–3515.
39 A. Ghorbanpour, A. Gumidyala, L. C. Grabow, S. P. Crossley and J. D. Rimer, Epitaxial Growth of ZSM-5@Silicalite-1: A Core-Shell Zeolite Designed with Passivated Surface Acidity, *ACS Nano*, 2015, **9**(4), 4006–4016.
40 C. F. Wang, L. Zhang, X. Huang, Y. F. Zhu, G. Li, Q. F. Gu, J. Y. Chen, L. G. Ma, X. J. Li, Q. H. He, J. B. Xu, Q. Sun, C. Q. Song, M. Peng, J. L. Sun and D. Ma, Maximizing sinusoidal channels of HZSM-5 for high shape-selectivity to p-xylene, *Nat. Commun.*, 2019, **10**, 4348–4356.
41 W. J. Meng, J. J. Li, F. C. Chen, S. J. Xie, S. G. Li, L. Y. Xu, X. J. Li and X. X. Zhu, An efficient synthesis protocol of core-shell ZSM-5@Silicalite-1 for the targeted alkylation reaction of toluene with ethanol, *Microporous Mesoporous Mater.*, 2024, **376**, 113183.
42 W. Dai, G. Wu, L. Li, N. Guan and M. Hunger, Mechanisms of the Deactivation of SAPO-34 Materials with Different Crystal Sizes Applied as MTO Catalysts, *ACS Catal.*, 2013, **3**, 588–596.
43 P. Liu, J. Han, L. Ling, X. Shen, P. Liu, R. Zhang and B. Wang, Correlation of Brønsted acid strengths and species substituted Si in ZSM-5 and their effects on propylene polymerization in MTA reaction, *Microporous Mesoporous Mater.*, 2023, **347**, 112346.
44 M. Srasra, S. Delsarte and E. M. Gaigneaux, Nitrided Zeolites: A Spectroscopic Approach for the Identification and Quantification of Incorporated Nitrogen Species, *J. Phys. Chem. C*, 2010, **114**, 4527–4535.
45 M. Shete, M. Kumar, D. Kim, N. Rangnekar, D. D. Xu, B. Topuz, K. V. Agrawal, E. Karapetrova, B. Stottrup, S. Al-Thabaiti, S. Basahel, K. Narasimharao, J. D. Rimer and M. Tsapatsis, Nanoscale Control of Homoepitaxial Growth on a Two-Dimensional Zeolite, *Angew. Chem., Int. Ed.*, 2017, **56**, 535–539.
46 Z. C. Shan, H. Wang, X. J. Meng, S. Y. Liu, L. Wang, C. Y. Wang, F. Li, J. P. Lewis and F. S. Xiao, Designed synthesis of TS-1 crystals with controllable b-oriented length, *Chem. Commun.*, 2011, **47**, 1048–1050.